Topological structures of river networks and their regional-scale controls: a multivariate classification approach

Yasmin Walley[1], Alexander J. Henshaw[1], James Brasington[2]

[1]School of Geography, Queen Mary, University of London, London, E1 4NS, United Kingdom
[2]Waterways Centre for Freshwater Management, University of Canterbury, Christchurch, New Zealand

Correspondence to: Yasmin Walley (y.r.s.walley@qmul.ac.uk)

Running Head: Topological structures of river networks

Article accepted for publication in Earth Surface Processes and Landforms on 16th June 2020

Abstract

Landscape evolution is governed by the interplay of uplift, climate, erosion, and the discontinuous pattern of sediment transfer from the proximal source of erosion to distal sedimentary sinks. The transfer of sediment through the catchment system is often referred to as a cascade, the pattern of which is modulated by the interaction of key network characteristics such as the distribution of transport capacity and resultant zones of sediment storage. An understanding of how sediment production is modulated through river networks with different topological structures at the associated timescales has remained elusive but presents significant implications for the knowledge of river response to disturbance events, and floodplain asset management.

A multivariate method of identifying representative topological structures from a range of river networks is presented. Stream networks from 59 catchments in the South Island of New Zealand were extracted from a Digital Elevation Model and their key topological parameters quantified. A principal component analysis was implemented to reduce these to two dimensional axes that represent the magnitude of network branching and the topographic structure of each catchment, respectively. An agglomerative hierarchical clustering analysis revealed five network 'types', which are examined in terms of their internal structural characteristics and relationships to potential regional-scale controls. Implications for sediment transfer in these network 'types' and their use as representative networks for further analysis are discussed.

Keywords

River Networks, Topology, Multivariate Analysis, Fluvial Systems, Sediment Transfer

1 Introduction

The processes that control the flux and storage of sediment have been widely researched at a variety of spatial and temporal scales, however an understanding of how these processes operate across entire drainage networks remains elusive. Previous research has focussed on the transfer of individual grains, the movement of sediment pulses through a reach (e.g. Lisle *et al.*, 2001; James, 2010) and the impact of intersecting tributaries (e.g. Knighton, 1980; Rice, 1998), with relatively few aiming to develop our understanding at the catchment scale. Understanding the discontinuous pattern of sediment routing through river networks is key to estimating spatial and temporal responses to significant disturbance events (Benda and Dunne, 1997b; Lisle *et al.*, 2001). Extreme disturbance events can result in landslide dams (e.g. Costa and Schuster, 1988; Hewitt, 2002; Korup, 2012; Kaiser *et al.*, 2017), significant aggradation leading to channel avulsion (Miller and Benda, 2000; e.g. Clague, Turner and Reyes, 2003; Korup, 2005), habitat degradation and loss of geoecological heterogeneity of the valley floor (Nakamura, Swanson and Wondzell, 2000; e.g. Geertsema, Schwab and Evans, 2006; James, 2010), and sediment contamination and reductions in water quality (Lin *et al.*, 2008; e.g. Geertsema, Highland and Vaugeouis, 2009). The propagation of effects downstream presents a secondary risk of bank erosion and flooding, often causing damage to local infrastructure in low-lying areas (Davies and Scott, 1997; e.g. Anthony and Julian, 1999; Geertsema, Schwab and Evans, 2006). As such, it is vital to address the role that river systems play in controlling the episodic behaviour of sediment transfer, and thus the impact of individual and coincident sediment pulses.

At the catchment scale, network configuration becomes a significant control on the modulation of sediment flux in river systems (Benda and Dunne, 1997b, 1997a; Benda, Andras, *et al.*, 2004; Benda, Poff, *et al.*, 2004; Benda, 2008; Ferguson and Hoey, 2008). This is particularly evident at confluence zones, in which the morphology reflects the relative flow and sediment inputs from the converging tributaries, as well as the episodic nature of sediment supply (Knighton, 1980; Benda and Dunne, 1997a; Rice, 1998; Benda, 2008). Each reach in a network converges with another of variable scale, forcing an interaction between regimes with different characteristics and magnitudes. Zones of significant sediment convergence and aggradation are interspersed with reaches of efficient routing to produce a pattern of discontinuous downstream transport, a pattern controlled by the configuration of effective and ineffective tributaries (Rice, 1998). Recent research in this area has centred on geomorphic 'hotspots' as key nodes in the river network predisposed to changes in storage and geomorphic change (Czuba and Foufoula-Georgiou, 2014, 2015; Walley, Tunnicliffe and Brierley, 2018).

Over much longer timescales, the same processes which control regional sediment transfer also determine the topology of river networks at the catchment scale. Tectonic and climatic settings establish topology during initial mountain building, and continue to evolve networks over time (Hovius *et al.*, 1998; Castelltort *et al.*, 2012). Complex relationships exist between regional setting, topology and sediment regimes, and the spatial and temporal scales over which these processes occur make them difficult to understand or quantify. The purpose of this study is to better understand the variation in topology across a range of river networks, and how this relates to regional setting/processes. Networks are classified into topological 'types' within the South Island of New Zealand, identifying and defining the range of topology across the region. The resulting classes represent a 'snapshot' of regional topology, allowing insights into the relationship between regional setting and network configuration, and establishing representative catchments for future regional-scale studies.

2 Regional Setting

The South Island of New Zealand is a highly dynamic landscape, in which active tectonics, weak lithology, high rates of rainfall and alpine processes at altitude combine to produce some of the highest rates of sediment production in the world (Milliman and Meade, 1983). The Southern Alps dominate the landscape, running the length of the island and rising to over 3000 m.a.s.l. at multiple locations (Fig. 1a) (Tippett and Kamp, 1995; Cook, Quincey and Brasington, 2014). The ridgeline is referred to as the 'Main Divide', separating Westland from the Canterbury Plains, and experiences rapid tectonic uplift (8-10 mm/yr) (Tippett and Kamp, 1993, 1995; Chamberlain *et al.*, 1999) and extremely high precipitation (14 m/yr) (Henderson and Thompson, 1999). The Southern Alps have a history of extensive glaciation, leading to the development of large, overwidened parabolic valleys and widespread alluvial megafans in the piedmont plains, exemplified by the Canterbury Plains. The dramatic topography of the South Island generates substantial diversity in the region's fluvial environments, particularly between the east and west coasts.

The landscape of New Zealand is intrinsically linked to deformation along the Australia-Pacific plate boundary (Fig. 1a). The westward subduction of the Pacific plate beneath the Australian plate off the east coast of the North Island, and the eastward subduction of the Australian Plate beneath the Pacific plate off the southern coast of the South Island, are linked along the by an oblique compressional zone of active continent-continent convergence (Tippett and Kamp, 1993; Davey *et al.*, 1998; Chamberlain *et al.*, 1999; Sutherland, Davey and Beavan, 2000; Craw *et al.*, 2013; Duvall *et al.*, 2019). This section of the plate boundary, the Alpine Fault, runs the length of the South Island and has resulted in the uplift of the Southern Alps (Fig. 1b). At the northern end of the Alpine Fault where plate collision transitions into subduction, the

Marlborough Fault System (MFS) is characterised by a set of predominantly strike-slip faults splaying north-eastward (Fig. 1a), which have also caused the uplift of linear mountain ranges (Craw *et al.*, 2013; Duvall *et al.*, 2019).

The Alpine Fault also divides the basement geology of the island into the Western and Eastern Provinces (Fig. 1b). The Western Province comprises quartz-rich metamorphic and intrusive igneous rocks of Paleozoic-Mesozoic age (Buller-Takaka Terrane), intruded by Median Batholith granites in the Devonian and Early Cretaceous (Davey *et al.*, 1998; Mortimer, 2004; Cox and Barrel, 2007; Shulmeister *et al.*, 2009). The Eastern Province comprises successive terranes of largely low-grade metasediments from the Permian-Jurassic period (Fig. 1b), which are being upthrust along the Alpine Fault (Davey *et al.*, 1998; Shulmeister *et al.*, 2009). Rapid uplift of marine sediments close to the fault has formed a band of highly metamorphosed schists (Grapes and Watanabe, 1992; Shulmeister *et al.*, 2009), the grade decreasing eastward to relatively unaltered greywacke within 15km of the fault (Davey *et al.*, 1998; Shulmeister *et al.*, 2009). A 460 km offset of the terranes along the Alpine Fault (Fig. 1b), and the rapid uplift of the Southern Alps mountain range reflects the highly active nature of the boundary (Tippett and Kamp, 1995; Chamberlain *et al.*, 1999; Sutherland, Davey and Beavan, 2000). Numerous branching faults cross the entirety of the South Island (Fig. 1a), and tectonics have consequently played a significant part in the shaping of the landscape (Tippett and Kamp, 1993, 1995; Sutherland, Davey and Beavan, 2000).

[Insert Figure 1 here]

The dominant topography of the Southern Alps plays a significant role in the pattern of regional climates across the South Island. The mountain range is oriented near-perpendicular to the prevailing westerly winds coming off the Tasman Sea, forcing strong orographic rainfall and a subsequent extensive rain shadow (Fig. 2a) (Griffiths and McSaveney, 1983; Chamberlain *et* *al.*, 1999; Sturman and Wanner, 2001; Craw *et al.*, 2013). The forcing of rapidly rising air over the Alps causes an average of 12 m of rainfall a year on the West Coast, compared to less than 1 m/yr on the East Coast (Griffiths and McSaveney, 1983; Craw *et al.*, 2013). The rain shadow is particularly pronounced in inland Central Otago, as Easterly and Southerly weather systems can increase rainfall along the eastern coastline (Craw *et al.*, 2013). The rainfall gradient can be exacerbated by the El Niño Southern Oscillation (ENSO), particularly in winter months (Golledge *et al.*, 2012).

The Last Glacial Maximum in New Zealand occurred approximately 28-18,000 yrs BP (Alloway *et al.*, 2007; Golledge *et al.*, 2012), and was characterised by cooling of >6 °C, a fall of typically 25% in annual precipitation (Golledge *et al.*, 2012). The Southern Alps during this period were covered in an elongate ice field, extending to sea level at points along the West Coast (Golledge *et al.*, 2012). Rapid warming during the Late Glacial (14,000-10,000 yrs BP) led to glacial retreat, which continued into the early Holocene, until approximately 6000 yrs BP (Leckie, 2003). A resurgence of small glacial events at around 5000 yrs BP occurred before the modern climate was established by 2500 yrs BP (Salinger and McGlone, 1990). The most recent maximum extension of glaciers in the Southern Alps was in the Little Ice Age (LIA) in the 17th-19th Centuries (Chinn *et al.*, 2005; Dykes and Brook, 2010). This was followed by a warming period between 1910-1970, in which glaciers retreated (Dykes and Brook, 2010). Historically, the glaciation of the Southern Alps has exacerbated erosion in the region and resulted in significant volumes of sediment transported downstream (Wilson, 1989; Leckie, 2003; Rowan *et al.*, 2012). The Last Glacial Maximum was associated with lower temperatures and precipitation, decreased vegetation cover and consequent erosion in the headwaters and fluvial aggradation (Leckie, 2003). This was particularly significant on the East Coast, as glacial outwash from the major rivers formed wide valley floors, braided river morphology, and megafans, eventually coalescing to form the Canterbury Plains (Leckie, 2003; Rowan *et al.*, 2012).

Patterns of land use are influenced by a number of factors, including geology, topography climate and access to water, as well as economic and societal pressures (Journeaux *et al.*, 2017). These factors are evident in the bands of land use identifiable in Fig. 2b, which correspond to patterns of geology, relief and rainfall. The steep slopes on the west coast are largely covered by indigenous forest, with pockets of grassland along flat valley floors. Pockets of exotic forest are also evident, indicating forestry activity in the region. The highest altitudes are mostly untouched by human activity, and are covered in permanent snow and ice, and exposed sediments. The Eastern High Country is a mixture of grassland and tussock grassland, typically used for extensive agriculture, compared to the gentle gradients on the east coast, which are largely grassland and cropland, with pockets of exotic forest. Similar regions were identified by Harding and Winterbourn (1997) in a classification of 'ecoregions' based on climate, rainfall, relief, vegetation, soils and geology. The multivariate comparison identified two primary clusters: native forest and high rainfall on the west coast, and tussock grassland, pasture and lower rainfall on the east coast. The classification also identifies eastern regions as being impacted more by human modification compared to the west coast.

[Insert Figure 2 here]

Regional controls produce distinctly different fluvial environments across the South Island. Particularly pronounced is the divide between the West and East coasts, in which the Alpine Fault, and consequently the Southern Alps, force strong contrasts in lithology, topography and climate. The western flanks of the Southern Alps descend steeply from the main divide, with glacial moraines creating interfluves between catchments and outwash plains extending to the coast (Shulmeister *et al.*, 2009). Rivers on these slopes are steeper, with coarser gravel beds which occupy gorges for much of their extent (Griffiths, 1979). The catchments are shorter, more closely spaced, and oriented sub-perpendicular to the Alpine Fault, compared to the long, generally oblique catchments to the east (Castelltort *et al.*, 2012). Rivers on the eastern slopes of the Southern Alps descend from steep eastern headwaters into highlands of intermontane basins and extensive piedmont plains. A distinct, although lesser contrast can be defined in the region of South Canterbury and Otago, in which the pronounced rain shadow effects and anthropogenic influence have significantly impacted sedimentary regimes. This region is also underlain by Otago Schist which is weaker than the surrounding greywacke, generating complex topography and concentrating drainage into the Clutha River catchment (Craw *et al.*, 2012). The transition of subduction to convergence within the MFS (Fig. 1a) has produced another fluvial environment, characterised by long, linear valleys and drainage anomalies, driven by uplift, deformation and river capture (Duvall *et al.*, 2019). These distinct regional settings produce variations in the hydraulic and sedimentary regimes of each area. In addition, agriculture, forestry and various forms of mining are key contributors of anthropogenic sediment, the extent of which depends on the methods and controls used (Ryan, 1991). Extensive hydraulic dam networks, particularly in South Canterbury and Otago, are also potentially contributors to anthropogenic sedimentary regimes, although many are constructed downstream of lakes and reservoirs limiting their impact on sediment regimes (Jowett, 1984). Very few studies have been conducted or published on the specific sources or impacts of anthropogenic sediment in New Zealand, and their role in the evolution of existing catchments is therefore not well understood (Ryan, 1991; Harding and Boothroyd, 2004).

3 Topological Classification

3.1 Network Extraction

Catchment boundaries for the entire South Island were extracted from a mosaicked 8 m Digital Elevation Model (DEM) originally produced from 1:50,000 topographic data (Geographx, 2012). Polygons in the centre of the island were clipped to the piedmont of the Southern Alps to remove lowlands in which clear drainage networks were not identifiable. River networks in catchments with an area larger than 300 km^2 were extracted in MATLAB using the TopoToolbox software

(Schwanghart and Kuhn, 2010; Schwanghart and Scherler, 2014) and the method outlined by Tarboton et al. (1991, 1992). The definition of 1st order reaches and hillslope units is problematic, particularly in disturbed landscapes where small channels, rills and gully systems can extend beyond the confines of the valley network (Montgomery and Dietrich, 1994). This is further exacerbated at a regional scale, in which area-only thresholds produce variable accuracy between different catchments. Figure 3 outlines Tarboton's method for extracting river networks.

[Insert Figure 3 here]

The DEM was initially processed by filling sinks and establishing flow direction within the catchment. A Peucker-Douglas Skeleton was generated based on the method of Peucker and Douglas (1975), creating a skeleton of the stream network based on grid cells with upward curvature. This skeleton was applied to a contributing area raster as a weighted input, and the resulting raster used to calculate a stream drop analysis based on the work of Broscoe (1959). The stream drop analysis calculates the statistical significance of a number of accumulation threshold values, from which the optimal value was identified as the most statistically significant difference between the drop in elevation of 1st order streams compared to those of higher order (Tarboton, Bras and Rodriguez-Iturbe, 1991, 1992). Stream drop thresholds were calculated for each of the 59 catchments, and the optimal values used to extract a link-based vector network from the weighted contributing area raster. A numerical connectivity structure was generated for each network, in which each link is assigned an ID and connected to the IDs of the two upstream links and the link immediately downstream.

3.2 Topological Metrics

A number of methods exist for characterizing the topology of river networks, which typically employ a number of metrics to capture the spatial distribution of links (e.g. Benda, Poff, *et al.*, 2004; Zanardo, Zaliapin and Foufoula-Georgiou, 2013; Heasley, Clifford and Millington, 2019). Previous studies have focussed on one of these variables (Strahler, 1957; e.g. Shreve, 1967; Zanardo, Zaliapin and Foufoula-Georgiou, 2013), or encompassed several within conceptual frameworks (e.g. Benda, Poff, *et al.*, 2004). More recently, studies have compared a number of quantitative metrics within several catchments, relating the internal structure to patterns of hydrology and sediment flux (Sklar *et al.*, 2016; Heasley, Clifford and Millington, 2019). Classifying the topological structures of the South Island region however, required the identification of a set of key topological metrics which encompassed the size, shape and internal branching structures, as well as enabled the calculation of a single representative value for each catchment (Table 1).

Four common variables of network topology were initially identified as Strahler Order, Shreve magnitude, drainage density and confluence angle (Strahler, 1957; Shreve, 1967; Benda, Poff, *et al.*, 2004). Strahler order in particular is frequently used in reach- and catchment-scale applications as a measure of network magnitude, and drainage density is often calculated to establish the level of landscape dissection (Benda, Poff, *et al.*, 2004; Heasley, Clifford and Millington, 2019). Values for Strahler order and Shreve magnitude were taken from the outlet, and drainage density was calculated for each network as the total network length divided by catchment area. The values of Shreve magnitude were later removed from the classification, as a Spearman's correlation matrix did not identify the variable as statistically significant. Confluence angles were calculated for each junction in the network following the method outlined by Seybold et al. (2017), and the mean value of all confluences taken as a representative value for each catchment.

The four identified variables establish the magnitude of network structure, but do not account for the spatial arrangement of links or the internal topography of each catchment. A value of network branching was thus calculated using Tokunaga's (1978) methodology, further developed by Tarboton (1996), Cui et al. (1999) , Zanardo et al. (2013), Danesh-Yazdi et al. (2017) and Walley et al. (2018). The *c* value (also referred to as *K* in other literature) is a measure of change in the average degree channel bifurcation between all Strahler Orders, such that links with 'self-similar' branching upstream (e.g. dendritic patterns) exhibit smaller values than those with long mainstems bounded by small tributaries (e.g. trellis patterns). A full description of this method is outlined in Walley et al. (2018). Two final values were calculated using catchment width and elevation, in order to capture the internal topography. Similar to the method of Heasley et al. (2019), each catchment was divided into 20 bands representing 5% of the total flow distance to the outlet. The number of links (by midpoint) and the mean elevation were calculated in each band, and the ratio between the 16^{th} and 84^{th} percentile calculated as representative values of catchment shape.

[Insert Table 1 here]

3.3 Classification

Principal Component Analysis (PCA) was used to explore topological relationships between the selected variables and reduce dimensionality. Two significant components were identified from a Spearman's correlation matrix, with eigenvalues greater than 1 and each representing more than 20% of the variance (Fig. 4a). The loading values for each of the original parameter values are included in Table 1, and their correlations with the two principal components is displayed in Fig. 4b.

[Insert Figure 4 here]

The two principal components were used to perform an Agglomerative Hierarchical Clustering analysis (AHC), using the Euclidean dissimilarity distance measure. Results obtained using five different linkage methods (complete, flexible, weighted, unweighted and Ward's) were compared, and clusters established based on membership consistency (Fig. 5a). The groupings were validated using the *k*-means clustering method as a comparison (Fig. 5b), which produced very similar clusters to the AHC method with the exception of cluster D. This disparity was attributed to the relatively small size of cluster D, and the tendency of the *k*-means method to produce spherical clusters of similar sizes due to the use of Voronoi cells in their calculation. Removing the three observations in cluster D thus furthers the validation of the other classes (Fig. 5c), although given that there is no reason to assume topologically comparable networks would occur in similar numbers across a given landscape, these networks were not excluded from further analysis. Kruskal-Wallis with Dunn's multiple comparison tests were thus performed on the AHC clusters, revealing statistically significant differences ($p < 0.0001$). Box-and-whisker plots of factor scores along the two primary components also show significantly distinct groupings, in which clusters with overlapping score ranges in one principal component, do not indicate any overlap in the second (Fig. 6).

[Insert Figure 5 here]

[Insert Figure 6 here]

3.4 Topological 'Types'

The five clusters of catchments thus identify 'types' of networks based on their topological characteristics. Each class represents a subset of the original parameters (Table 2), as identified by the loading value for each primary component (Fig. 4b). The first component (PC1) is linked to Strahler order, network branching (*c* value) and width ratios, and thus was interpreted to represent variance in network structure. The second component (PC2) is linked to elevation ratios, drainage density and confluence angles, and was interpreted to represent variance in topography. Catchments in classes A to E therefore exhibit decreasing size and increasing values of network branching, with a shift from catchment shapes with wide headwaters to those of more consistent widths (Table 2; Fig. 4b). Along PC2, drainage density and elevation difference are greatest in classes B and E, while class D includes networks with the largest confluence angles.

The greatest contrast in topological 'types' is therefore evident between diagonally opposite classes, i.e. A and E, B and D (Fig. 5a; Table 2). Catchments in class A tend to be larger, with much of the catchment area occurring furthest from the outlet and narrowing with distance. Elevation differences and drainage density are moderate, with relatively large catchment angles. In contrast, class E catchments are much steeper, smaller, and have a consistent width with distance from the outlet. The networks are more structured than Class A, and contain smaller confluence angles. Class B is similar to class A in that the networks are larger and less structured, with a mix of catchments exhibiting wide headwaters and consistent widths. The topology is closer to class E along the secondary component, exhibiting steeper elevation differences, high drainage density and smaller confluence angles. Finally, Class D shares greater similarity with class E along component 1 and class A along component 2, in direct contrast to class B. The networks in class D exhibit the greatest degree of network branching and largest catchment angles, within smaller catchments of consistent width.

[Insert Table 2 here]

4 Internal Network Structure

To identify the type of networks in each class, it is necessary to explore properties not included in the original parameters. The PCA/AHC method necessarily reduces variables of topology to single values, thus does not account for internal variability within each catchment. The exception to this is the c value, the calculation of which is designed to represent the cumulative magnitude of upstream network branching (Tokunaga, 1978; Walley, Tunnicliffe and Brierley, 2018). Sklar et al. (2016) considers catchments as a collection of point locations, in which each point can be attributed with individual values for a variety of variables. Their methods of displaying elevation, travel distance and slope variables are employed in order to better understand the internal topological variability within each catchment, and within the identified classes. In order to clearly draw comparisons between each of the classes, the objects closest to the centroid of each cluster were identified as representative of network topologies in that group. The catchments are presented in order through Figs. 7, 8 and 9, such that panels a-e in each figure corresponds to the associated class.

Network maps (Fig. 7a-e) and width functions (Fig. 7f-j) exhibit the Strahler magnitudes and planform structure for each of the central objects. Notably, classes A and B contain catchments with more rounded shapes, compared to the elongate shapes in D and E, which corresponds to the trends in the width functions. For example, the distribution for the Arahura River (Fig. 7j) is symmetrical with a low peak, reflecting the rectangular shape of the catchment. In contrast, most of the area in the Motueka River (Fig. 7f) occurs in the upper half of the catchment, reflecting the narrowing towards the outlet. These differences in planform structure reflect the distribution of catchments along PC1 (Fig. 4b), and thus corresponds to c values for each catchment, which are much larger in classes D and E. Network maps also display a shift in scale corresponding to the Strahler value, as catchments in classes A and B tend to be larger than those in D and E. Note that for each variable, catchments in class C tend to reflect a mixture of characteristics of the other classes.

[Insert Figure 7 here]

Figure 7 also includes hypsometry functions, generated in the same manner as the width functions. In contrast to the network structure variables, elevation varies along PC2 (Fig 4b), thus classes B and E exhibit very similar trends in which most of the catchment area occurs at low elevations. Catchment area in classes A and D subsequently occurs at low-mid elevations in relatively normal distributions. To further explore patterns of topography, bivariate frequency distributions of elevation and travel distance for every point in each catchment (Point Area = 50 km^2) were generated in the manner of Sklar et al. (2016) (Fig. 8 a-j). Values of point density were additionally mapped onto the original catchment grid to explore the spatial distribution of high density areas (Fig. 8k-o). The areas of highest density in classes B and E occur along the valley floor in areas of minimal elevation change, corresponding to the trends observed in the hypsometry functions. Of note however, is that these flat areas in class B tend to occur toward the centre of the catchment, while they are closer to the outlets in class E. In contrast, class A catchments exhibit the highest point density along tendrils which curve away from the valley floor, indicating that elevation increases at a similar rate with distance from the outlet in multiple parts of the catchment. As can be observed in the map of the Motueka catchment (Figure 8k), these patterns indicate a topographic symmetry of the valley floor upstream of certain outlets, in which elevation increases with travel distance at a similar rate along the upstream links.

[Insert Figure 8 here]

The topographic patterns observed in the bivariate frequency distributions are reinforced by the spatial distributions of mean slope, calculated as the ratio of elevation and travel distance at every point in each catchment (Fig. 9f-j). Common values appear as linear trends through the distributions of travel distance and elevation (Fig. 9a-e) and as contours when mapped onto the original catchment grid (Fig. 9k-o) (Sklar *et al.*, 2016). Classes B and E both include catchments with very steep (e.g. Arahura River) and very gentle (e.g. Tokomairiro River) gradients. The former trend occurs in catchments located on the west coast of the South Island, where the topography of the Southern Alps forces very steep changes in elevation over relatively short distances. The histograms reflect the greater range in slopes occurring at lower frequencies

(Fig. 9j), which also tend to include a high frequency bar at a very low slope value. In contrast, the catchments with more gentle gradients tend to produce left-skewed histograms, many of which have only a few very high frequency bars at low slopes (Fig. 9g). These catchments tend to be found on the east and south coasts of the South Island, where they occupy a much larger land area than those on the west coast or do not extend to the main divide of the Southern Alps. Classes A and C include catchments with low-moderate elevation change, occurring over greater distances than classes B and E. Histograms are more normally distributed, with moderate frequency peaks (Fig. 9f). A few distributions extend into greater slopes, these tend to occur where relatively high elevations occur towards the catchment outlet (Fig. 9h). Note that no trend was identifiable in Class D for mean slope, given the small size of the group.

Contour maps (Fig. 9k-o) reflect the trends in topography observed in the bivariate frequency distributions (Fig. 8). Classes B and E include areas of very flat topography, occurring toward the outlets in class E (Fig. 9o), and in the centre of the catchments in class B (Fig. 9l). Class A exhibits steady elevation-distance relationship in multiple links (Fig. 9k). These maps additionally highlight the network structure trends, in which catchments in classes A and B contain dissected networks, while those in classes D and E exhibit prominent central mainstems.

[Insert Figure 9 here]

5 Evaluation

The relationship between each class and the principal components is summarized in Fig. 10. Class A contains large, wide catchments with dissected network structures, situated on low-moderate slopes in which elevation tends to increase constantly with distance from the outlet. Class B also contains catchments with dissected network structures, however they are more elongate than those in Class A, including a mixture of sizes and very steep and gently sloped gradients. These catchments tend to include areas of very flat topography toward the middle reaches. Class C depicts no clear trend, instead the networks reflect a mixture of topologies, with elements from the other classes. Catchments in Class D exhibit significant structural influence, with smaller, elongate shapes on moderately steep slopes, and clear mainstem-dominated networks. Class E catchments are similar to Class D but occur across steeply sloping gradients and tend to have large flat areas of topography at the outlet.

[Insert Figure 10 here]

Patterns of topology in the South Island are determined by a complex interplay of tectonic, climatic and erosional evolution, potentially dating back to before the initial uplift of the Southern Alps (Castelltort and Simpson, 2006; Willett *et al.*, 2014; Viaplana-Muzas *et al.*, 2015). Studies have suggested that drainage networks in mountain ranges are established during initial collision and uplift (Hovius *et al.*, 1998; Castelltort and Simpson, 2006; Viaplana-Muzas *et al.*, 2015), but the influence of regional setting on subsequent evolution is relatively unknown. Rather than analysing the relationship of a single network with its regional controls, the identification of topological 'types' enables an analysis of how elements of regional setting are distributed across groups of networks with similar characteristics. South Island datasets of estimated uplift, average annual rainfall and suspended sediment yield were thus used to represent regional setting, and box-and-whisker plots were generated from the mean values from each catchment (Fig. 11).

[Insert Figure 11 here]

Active mountain regions like the Southern Alps exhibit ongoing tectonic movement, driving reorganisation of established river networks through river capture, catastrophic landsliding, and passive deformation (Hovius *et al.*, 1998; Castelltort *et al.*, 2012). Uplift processes thus strongly influence the patterns of drainage networks in the region, as evidenced by Fig. 11a. Classes A to E exhibit ranges of uplift rates and stepped increases in mean value, which is similar in classes A and B, C and D and much greater in class E. This pattern is driven by the multitude of small class E catchments along the west coast of the South Island (Fig. 12a), which are intersected by the underlying Alpine Fault (Fig. 12b). The high rates of uplift in class E (Fig. 11a) thus suggest a correlation between tectonics and topological network structure (Fig. 10), with mainstem-dominant networks more strongly influenced by tectonic activity.

The Alpine Fault is an oblique-dextral fault in which the Pacific Plate in the east is ramping up against the western Australian Plate (Davey *et al.*, 1998; Sutherland, Davey and Beavan, 2000; Duvall *et al.*, 2019). The western flanks of the Southern Alps are consequently much narrower than those to the east, limiting the available space for headwater extension and network growth, and giving rise to multiple small networks of classes B and E spanning from the Main Divide to the coast (Fig 11a). The size of these catchments and the offset of the Alpine Fault from the Main Divide, cause entire networks to be in close proximity to the rapid uplift along the alpine fault, driving dynamic reorganisation in response to tectonic strain through river capture and catastrophic landsliding (Castelltort *et al.*, 2012). It is also likely that the multitude of faults across the South Island may impose network orientation along weak structures (Craw, Youngson and Koons, 1999; Castelltort *et al.*, 2012; Kirby, 2012), which is evident in the MFS (Fig. 1a), which contains a number of main-stem dominant networks aligned with underlying faults (Duvall *et al.*, 2019).

Uplift along the Alpine Fault additionally gives rise to the Southern Alps, which transect the prevailing westerly winds and generate a strong orographic rainfall gradient across the South Island (Fig. 2a). This rainfall gradient is reflected in the distribution of rainfall across the topological classes (Fig. 11b), in which class E catchments on the west coast are significantly wetter than those in other classes. The distribution of rainfall is similar to that of specific suspended sediment yield (Fig. 11c), reflecting the correlation between sediment transport and discharge. Both graphs indicate higher values in class E, driven by the prevalence of small, steep west coast catchments, underlain by weak geology crushed by the active tectonics.

In contrast, the other classes exhibit relatively low mean values of rainfall and specific suspended sediment yield, reflecting the relatively dry environments across the rest of the South Island (Fig. 2a). Class A exhibits a relatively narrow range of low rainfall values, which reflects the prevalence of these catchments on the eastern and northern coasts of the South Island (Fig. 12a). Combined with the relatively weak geology and availability of space due to the position of the Alpine Fault, these networks have likely grown through river capture and mass movement, evidenced by their relatively large sizes and wide headwater networks. This is particularly evident in the Clutha River, the largest catchment which occupies the area underlain by Otago Schist (Fig. 1b). It is possible that the size of the catchment has been exacerbated by the exceptionally weak geology and pronounced rain shadow. There is therefore no apparent connection between climate and rainfall as established by Seybold et al. [2017], who indicated that smaller confluence angles occur in more arid environments and increase with humidity. In contrast, the catchments in classes B and E contain the smallest confluence angles (Table 2) but exhibit distinctly different ranges of annual rainfall (Fig. 11b).

[Insert Figure 12 here]

Catchments in the same topological class are expected to exhibit common trends in patterns of sediment connectivity. The spatial arrangement of links within river networks concentrates the routing of sediment and water into parts of the catchment, often at particular confluences (Czuba and Foufoula-Georgiou, 2015; Walley, Tunnicliffe and Brierley, 2018; Heasley, Clifford and Millington, 2019). These 'hotspots' give rise to particularly dynamic tributary junctions, and there is some evidence to suggest that their location can be defined through network topology (Benda, Andras, *et al.*, 2004; Czuba and Foufoula-Georgiou, 2015; Czuba *et al.*, 2017; Walley, Tunnicliffe and Brierley, 2018). Highly dynamic tributary junctions can be expected to occur in all network types but will likely have varying impacts on the catchment-scale patterns of sediment flux. In catchments with wide headwater networks and large confluence angles such as those in Class A, hotspots are likely to occur where large sub-networks converge, and may have a primary role in modulating patterns of sediment routing through these networks (Czuba and Foufoula-Georgiou, 2015; Walley, Tunnicliffe and Brierley, 2018). Similar storage patterns have been observed in networks with wide headwaters (Fryirs and Brierley, 2001; e.g. Benda, Poff, *et al.*, 2004; Gran and Czuba, 2017), and at the head of mainstem channels in elongate catchments (e.g. Benda, Andras, *et al.*, 2004; Walley, Tunnicliffe and Brierley, 2018). In contrast, routing and storage behaviour in elongate networks exhibits sediment concentrated along valley floors, with rapid transport of sediment from adjacent hillslope tributaries (e.g. Benda, Andras, *et al.*, 2004; Farraj and Harvey, 2010; Walley, Tunnicliffe and Brierley, 2018). The structured, steep nature of catchments in classes D and E are therefore likely to reflect this pattern. Catchments in classes A and B may thus exhibit more sediment storage in upstream reaches compared to those in classes D and E, although storage in class B and E catchments are also likely to be controlled by the areas of flat topography.

Catchment-scale models would enable testing of these hypotheses and an exploration of the relationship between topology and sediment connectivity. In particular, the network-based framework model created by Czuba and Foufoula-Georgiou (2014, 2015) was designed for this purpose, as a system-level model without the pitfalls of reductionist approaches or over-parameterized physically based models. It is relatively new however, and model validation using real-world data is difficult given the spatial and temporal scales involved. Benchmarking the model against one known to accurately represent catchment-scale processes would address this issue and allow for an evaluation of both the topology-sediment connectivity relationship and the model itself. The topological classification presented here would thus define the regional topological ‘types’, as well as allow for a prioritised, representative selection of study catchments.

6 Conclusions

The regional topology of the South Island of New Zealand presents five distinct catchment ‘types’ based on six topological metrics. The variables were chosen to encompass the size and shape of catchments as well as the internal distribution of links, and the values for each catchment were calculated to enable the use of Principal Components Analysis (PCA) and Agglomerative Hierarchical Clustering (AHC). Each class comprises catchments of significantly different topography and network structure, with the greatest contrast observed between diagonally opposite clusters (Fig. 10). Class A includes large catchments with wide headwaters and confluence angles, and a high degree of valley-floor symmetry extending into the upper reaches of the catchment. Networks in class B are also large with a mixture of wide headwaters and consistent widths, but the topography tends to be steeper and include large areas of flat relief. Patterns of sediment routing in both classes are likely to be modulated by dynamic hotspots occurring at the confluences of large sub-networks. In contrast, catchments in classes D and E exhibit much greater structural influence on the arrangement of network links, encompassing smaller catchments of consistent widths. Confluence angles are particularly large in class D networks, while those in class E are steeper with greater drainage density. Sediment routing in these networks is therefore likely to be concentrated along the valley floors of mainstem reaches, with rapidly transported inputs from the adjacent hillslope tributaries.

The spatial distribution of classes within the South Island provides insight to the relationship between topology and regional setting, largely dominated by the active tectonics in the region. The offset of the Alpine Fault towards the west coast limits catchment size on the western flanks, and establishes differing patterns of dynamic reorganisation and passive deformation on each coast. The pattern of active faulting also has a clear influence on the structure and orientation of networks. The relationship between catchment-scale processes and regional setting is not well-understood, despite the clear influence of network configuration on the modulation of sediment flux (Benda and Dunne, 1997b, 1997a; Benda, Andras, *et al.*, 2004; Benda, Poff, *et al.*, 2004; Benda, 2008; Ferguson and Hoey, 2008). Establishing this relationship has particular implications for the South Island, as there is a high likelihood of widespread landsliding driven by significant tectonic shifts and large storm events. Further research into the patterns of sediment routing through topologically different networks will provide greater clarity on the potential impacts of these events, and the ongoing catchment management in the region.

Acknowledgments

We thank the editor (Stuart Lane) and Sarah Schanz for their comments, which helped to improve the manuscript. We thank the Otago Regional Council, Environment Canterbury and NIWA for supplying hydrological gauge data. This study was supported by funding from a Principal's Studentship at Queen Mary, University of London.

The authors declare that they have no conflict of interest.

Data Availability

The data sets used and/or analysed during the current study are available from the corresponding author on reasonable request.

Public data sources can be found at the following:

https://data.linz.govt.nz/layer/768.

https://www.gns.cri.nz/Home/Our-Science/Land-and-Marine-Geoscience/Regional-Geology/Geological-Maps/1-250-000-Geological-Map-of-New-Zealand-QMAP/Digital-Data-and-Downloads

https://data.mfe.govt.nz/layer/103686-updated-suspended-sediment-yield-estimator-and-estuarine-trap-efficiency-model-results-2019/.

https://lris.scinfo.org.nz/layer/48423-lcdb-v41-land-cover-database-version-41-mainland-new-zealand/.

https://data.mfe.govt.nz/x/UEXef3.

References

Alloway, B. V. *et al.* (2007) 'Towards a climate event stratigraphy for New Zealand over the past 30 000 years (NZ-INTIMATE project)', *Journal of Quaternary Science*. John Wiley & Sons, Ltd., 22(1), pp. 9–35. doi: 10.1002/jqs.1079.

Anthony, E. J. and Julian, M. (1999) 'Source-to-sink sediment transfers, environmental engineering and hazard mitigation in the steep Var River catchment, French Riviera, southeastern France', *Geomorphology*. Elsevier, 31(1–4), pp. 337–354. doi: 10.1016/S0169-555X(99)00088-4.

Benda, L., Andras, K., *et al.* (2004) 'Confluence effects in rivers: Interactions of basin scale, network geometry, and disturbance regimes', *Water Resources Research*, 40. doi: 10.1029/2003WR002583.

Benda, L., Poff, N. L., *et al.* (2004) 'The Network Dynamics Hypothesis: How Channel Networks Structure Riverine Habitats', *BioScience*, 54(5), pp. 413–427. doi: 10.1641/0006-3568(2004)054[0413:TNDHHC]2.0.CO;2.

Benda, L. (2008) 'Confluence environments at the scale of river networks', in Rice, S. P., Roy, A., and Rhoads, B. L. (eds) *River Confluences, Tributaries and the Fluvial Network*. Wiley & Sons Ltd., pp. 271–300.

Benda, L. and Dunne, T. (1997a) 'Stochastic forcing of sediment routing and storage in channel networks', *Water Resources Research*, 33(12), pp. 2865–2880.

Benda, L. and Dunne, T. (1997b) 'Stochastic forcing of sediment supply to channel networks from landsliding and debris flow', *Water Resources Research*, 33(12), pp. 2849–2863. doi: 10.1029/97WR02388.

Broscoe, A. (1959) *Quantitative analysis of longitudinal stream profiles of small watersheds*. New York. Available at: http://www.dtic.mil/get-tr-doc/pdf?AD=AD0233820 (Accessed: 18 August 2017).

Castelltort, S. *et al.* (2012) 'River drainage patterns in the New Zealand Alps primarily controlled by plate tectonic strain', *Nature Geoscience*. Nature Publishing Group, 5(10), pp. 744–748. doi: 10.1038/ngeo1582.

Castelltort, S. and Simpson, G. (2006) 'River spacing and drainage network growth in widening mountain ranges', *Basin Research*, 18(3), pp. 267–276. doi: 10.1111/j.1365-2117.2006.00293.x.

Chamberlain, C. P. P. *et al.* (1999) 'Topographic development of the Southern Alps recorded by the isotopic composition of authigenic clay minerals, South Island, New Zealand', *Chemical Geology*, 155(3–4), pp. 279–294. doi: 10.1016/S0009-2541(98)00165-X.

Chinn, T. J. H. *et al.* (2005) 'Recent glacier advances in Norway and New Zealand: A comparison of their glaciological and meteorological causes', *Geografiska Annaler, Series A: Physical Geography*, 87(1), pp. 141–157. doi: 10.1111/j.0435-3676.2005.00249.x.

Clague, J. J., Turner, R. J. W. and Reyes, A. V. (2003) 'Record of recent river channel instability, Cheakamus Valley, British Columbia', *Geomorphology*. Elsevier, 53(3–4), pp. 317–332. doi: 10.1016/S0169-555X(02)00321-5.

Cook, S. J., Quincey, D. J. and Brasington, J. (2014) 'Geomorphology of the Rees Valley, Otago, New Zealand', *Journal of Maps*, 10(1). doi: 10.1080/17445647.2013.863744.

Costa, J. E. and Schuster, R. L. (1988) 'The formation and failure of natural dams', *Geological Society of America Bulletin*. GeoScienceWorld, 100(7), pp. 1054–1068. doi: 10.1130/0016-7606(1988)100<1054:TFAFON>2.3.CO;2.

Cox, S. and Barrel, D. (2007) 'Geology of the Aoraki area, Institute of Geological and Nuclear Sciences 1: 250000', *Lower Hutt, New Zealand (GNS Science)*.

Craw, D. *et al.* (2012) ‘Tectonic controls on the evolution of the Clutha River catchment, New Zealand’, *New Zealand Journal of Geology and Geophysics*, 55(4), pp. 345–359. doi: 10.1080/00288306.2012.709184.

Craw, D. *et al.* (2013) ‘Geological controls on palaeo-environmental change in a tectonic rain shadow, southern New Zealand’, *Palaeogeography, Palaeoclimatology, Palaeoecology*. Elsevier B.V., 370, pp. 103–116. doi: 10.1016/j.palaeo.2012.11.024.

Craw, D., Youngson, J. H. and Koons, P. O. (1999) ‘Gold dispersal and placer formation in an active oblique collisional mountain belt, Southern Alps, New Zealand’, *Economic Geology*, 94(5), pp. 605–614. doi: 10.2113/gsecongeo.94.5.605.

Cui, G., Williams, B. and Kuczera, G. (1999) ‘A stochastic Tokunaga model for stream networks’, *Water Resources Research*, 35(10), pp. 3139–3147. doi: 10.1029/1999WR900168.

Czuba, J. A. *et al.* (2017) ‘Interplay between Spatially-Explicit Sediment Sourcing, Hierarchical River-Network Structure, and In-Channel Bed-Material Sediment Transport and Storage Dynamics’, *Journal of Geophysical Research: Earth Surface*. doi: doi: 10.1002/2016JF003965.

Czuba, J. A. and Foufoula-Georgiou, E. (2014) ‘A network-based framework for identifying potential synchronizations and amplifications of sediment delivery in river basins’, *Water Resources Research*, 50(5), pp. 3826–3851. doi: 10.1002/2013WR014227.

Czuba, J. A. and Foufoula-Georgiou, E. (2015) ‘Dynamic connectivity in a fluvial network for identifying hotspots of geomorphic change’, *Water Resources Research*, 51, pp. 1401–1421. doi: 10.1002/2015WR016967.

Danesh-Yazdi, M., Tejedor, A. and Foufoula-Georgiou, E. (2017) ‘Self-dissimilar landscapes: Revealing the signature of geologic constraints on landscape dissection via topologic and multi-scale analysis’, *Geomorphology*. Elsevier, 295, pp. 16–27. doi: 10.1016/J.GEOMORPH.2017.06.009.

Davey, F. *et al.* (1998) ‘Preliminary results from a geophysical study across a modern, continent-

continent collisional plate boundary — the Southern Alps, New Zealand', *Tectonophysics*. Elsevier, 288(1–4), pp. 221–235. doi: 10.1016/S0040-1951(97)00297-7.

Davies, T. R. and Scott, B. K. (1997) 'Dambreak flood hazard from the Callery River, Westland, New Zealand', *Journal of Hydrology (New Zealand)*. New Zealand Hydrological Society, pp. 1–13. doi: 10.2307/43944780.

Duvall, A. R. *et al.* (2019) 'River patterns reveal landscape evolution at the edge of subduction, Marlborough Fault System, New Zealand', *Earth Surface Dynamics Discussions*, pp. 1–28. doi: 10.5194/esurf-2019-41.

Dykes, R. C. and Brook, M. S. (2010) 'Terminus recession, proglacial lake expansion and 21st century calving retreat of Tasman Glacier, New Zealand', *New Zealand Geographer*. Blackwell Publishing Asia, 66(3), pp. 203–217. doi: 10.1111/j.1745-7939.2010.01177.x.

Farraj, A. AL and Harvey, A. (2010) 'Influence of hillslope-to-channel and tributary-junction coupling on channel morphology and sediments: Bowderdale Beck, Howgill Fells, NW England', *Zeitschrift für Geomorphologie*, 54(2), pp. 203–224. doi: 10.1127/0372-8854/2010/0054-0018.

Ferguson, R. I. and Hoey, T. B. (2008) 'Effects of Tributaries on Main-Channel Geomorphology', in Rice, S. P., Roy, A. G., and Rhoads, B. L. (eds) *River Confluences, Tributaries and the Fluvial Network*. John Wiley & Sons, Ltd, pp. 183–208.

Fryirs, K. A. and Brierley, G. J. (2001) 'Variability in sediment delivery and storage along river courses in Bega catchment, NSW, Australia: Implications for geomorphic river recovery', *Geomorphology*, 38, pp. 237–265. doi: 10.1016/S0169-555X(00)00093-3.

Geertsema, M., Highland, L. and Vaugeouis, L. (2009) 'Environmental Impact of Landslides', in Sassa, K. and Canuti, P. (eds) *Landslides - Disaster Risk Reduction*. Springer Berlin Heidelberg, pp. 589–607.

Geertsema, M., Schwab, J. W. and Evans, S. G. (2006) 'An overview of recent large catastrophic landslides in northern British Columbia, Canada', *Engineering Geology*. Elsevier, 83(1–3), pp. 120–143. doi: 10.1016/J.ENGGEO.2005.06.028.

Golledge, N. R. *et al.* (2012) 'Last Glacial Maximum climate in New Zealand inferred from a modelled Southern Alps icefield', *Quaternary Science Reviews*. Elsevier Ltd, 46, pp. 30–45. doi: 10.1016/j.quascirev.2012.05.004.

Gran, K. B. and Czuba, J. A. (2017) 'Sediment pulse evolution and the role of network structure', *Geomorphology*. Elsevier B.V., 277, pp. 17–30.

Grapes, R. and Watanabe, T. (1992) 'Metamorphism and uplift of Alpine schist in the Franz Josef?Fox Glacier area of the Southern Alps, New Zealand', *Journal of Metamorphic Geology*. Blackwell Publishing Ltd, 10(2), pp. 171–180. doi: 10.1111/j.1525-1314.1992.tb00077.x.

Griffiths, G. A. (1979) 'High sediment yields from major rivers of the Western Southern Alps, New Zealand', *Nature*, pp. 61–63. doi: 10.1038/282061a0.

Griffiths, G. A. and McSaveney, M. J. (1983) 'Distribution of mean annual precipitation across some steepland regions of New Zealand', *New Zealand Journal of Science*, 26(2), pp. 197–209.

Harding, J. S. and Boothroyd, I. (2004) 'Impacts of Mining', in Harding, J. et al. (eds) *Freshwaters of New Zealand*. Wellington: New Zealand Hydrological Society.

Harding, J. S. and Winterbourn, M. J. (1997) 'An Ecoregion Classification of the South Island, New Zealand', *Journal of Environmental Management*, 51(3), pp. 275–287. doi: 10.1006/jema.1997.0145.

Heasley, E. L., Clifford, N. J. and Millington, J. D. A. (2019) 'Integrating network topology metrics into studies of catchment-level effects on river characteristics', *Hydrology and Earth System Sciences*, 23(5), pp. 2305–2319. doi: 10.5194/hess-23-2305-2019.

Henderson, R. D. and Thompson, S. M. (1999) 'Extreme rainfalls in the Southern Alps of New Zealand', *Journal of Hydrology*, pp. 309–330.

Hewitt, K. (2002) 'Postglacial Landform and Sediment Associations in a Landslide-Fragmented River System: The Transhimalayan Indus Streams, Central Asia', in *Landscapes of Transition*.

Springer, Dordrecht, pp. 63–91. doi: 10.1007/978-94-017-2037-3_4.

Hovius, N. *et al.* (1998) 'Landslide-driven drainage network evolution in a pre-steady state mountain belt: Finisterre Mountains, Papua New Guinea', *Geology*, 26(12 (December)), pp. 1071–1074.

James, L. A. (2010) 'Secular Sediment Waves, Channel Bed Waves, and Legacy Sediment', *Geography Compass*, 4(6), pp. 56–598. doi: 10.1111/j.1749-8198.2010.00324.x.

Journeaux, P. *et al.* (2017) *Analysis of Drivers and Barriers to Land Use Change: A Report prepared for the Ministry for Primary Industries*.

Jowett, I. (1984) 'Sedimentation in New Zealand Hydroelectric Schemes', *Water International*, 9(4), pp. 172–176. doi: 10.1080/02508068408686533.

Kaiser, A. *et al.* (2017) 'The 2016 Kaikōura, New Zealand, Earthquake: Preliminary Seismological Report', *Seismological Research Letters*, 88(3), pp. 727–739. doi: 10.1785/0220170018.

Kirby, E. (2012) 'Geomorphology: Tectonically twisted rivers', *Nature Geoscience*. Nature Publishing Group, 5(10), pp. 688–689. doi: 10.1038/ngeo1594.

Knighton, A. D. (1980) 'Longitudinal changes in size and sorting of stream-bed material in four English rivers', *Geological Society of America Bulletin*, 91, pp. 55–62. doi: 10.1130/0016-7606(1980)91<55:LCISAS>2.0.CO;2.

Korup, O. (2005) 'Large landslides and their effect on sediment flux in South Westland, New Zealand', *Earth Surface Processes and Landforms*, 30(3), pp. 305–323. doi: 10.1002/esp.1143.

Korup, O. (2012) 'Earth's portfolio of extreme sediment transport events', *Earth-Science Reviews*. Elsevier, 112(3–4), pp. 115–125. doi: 10.1016/J.EARSCIREV.2012.02.006.

Leckie, D. A. (2003) 'Modern environments of the Canterbury Plains and adjacent offshore areas, New Zealand - An analog for ancient conglomeratic depositional systems in nonmarine and coastal zone settings', *Bulletin of Canadian Petroleum Geology*, 51(4), pp. 389–425. doi:

10.2113/51.4.389.

Lin, G.-W. *et al.* (2008) ‘Effects of earthquake and cyclone sequencing on landsliding and fluvial sediment transfer in a mountain catchment’, *Earth Surface Processes and Landforms*. John Wiley & Sons, Ltd, 33(9), pp. 1354–1373. doi: 10.1002/esp.1716.

Lisle, T. E. *et al.* (2001) ‘The dominance of dispersion in the evolution of bed material waves in gravel-bed rivers’, *Earth Surface Processes and Landforms*, 26(13), pp. 1409–1420. doi: 10.1002/esp.300.

Miller, D. J. and Benda, L. (2000) ‘Effects of punctuated sediment supply on valley-floor landforms and sediment transport’, *Geological Society of America Bulletin*. GeoScienceWorld, 112(12), p. 1814. doi: 10.1130/0016-7606(2000)112<1814:EOPSSO>2.0.CO;2.

Milliman, J. D. and Meade, R. H. (1983) ‘World-Wide Delivery of River Sediment to the Oceans’, *The Journal of Geology*. University of Chicago Press , 91(1), pp. 1–21. doi: 10.1086/628741.

Montgomery, D. R. and Dietrich, W. E. (1994) ‘Landscape Dissection and Drainage Area-Slope Thresholds’, in Kirkby, M. J. (ed.) *Process Models and Theoretical Geomorphology*. Wiley & Sons Ltd., pp. 221–246.

Mortimer, N. (2004) ‘New Zealand’s Geological Foundations’, *Gondwana Research*, 7(1), pp. 261–272. doi: 10.1016/S1342-937X(05)70324-5.

Nakamura, F., Swanson, F. J. and Wondzell, S. M. (2000) ‘Disturbance regimes of stream and riparian systems - a disturbance-cascade perspective’, *Hydrological Processes*. John Wiley & Sons, Ltd, 14(16–17), pp. 2849–2860. doi: 10.1002/1099-1085(200011/12)14:16/17<2849::AID-HYP123>3.0.CO;2-X.

Peucker, T. K. and Douglas, D. H. (1975) ‘Detection of Surface-Specific Points by Local Parallel Processing of Discrete Terrain Elevation Data’, *Computer Graphics and Image Processing*, 4, pp. 375–387. doi: 10.1016/0146-664X(75)90005-2.

Rice, S. P. (1998) ‘Which tributaries disrupt downstream fining along gravel-bed rivers?’, *Geomorphology*, 22, pp. 39–56. doi: 10.1016/S0169-555X(97)00052-4.

Rowan, A. V. *et al.* (2012) 'Optically stimulated luminescence dating of glaciofluvial sediments on the Canterbury Plains, South Island, New Zealand', *Quaternary Geochronology*. Elsevier B.V, 8(1), pp. 10–22. doi: 10.1016/j.quageo.2011.11.013.

Ryan, P. A. (1991) 'Environmental effects of sediment on New Zealand streams: A review', *New Zealand Journal of Marine and Freshwater Research*, 25(2), pp. 207–221. doi: 10.1080/00288330.1991.9516472.

Salinger, M. J. and McGlone, M. S. (1990) 'New Zealand Climate - The past two million years', *The New Zealand Climate Report*, pp. 13–17.

Schwanghart, W. and Kuhn, N. J. (2010) 'TopoToolbox: A set of Matlab functions for topographic analysis', *Environmental Modelling & Software*. Elsevier, 25(6), pp. 770–781. doi: 10.1016/J.ENVSOFT.2009.12.002.

Schwanghart, W. and Scherler, D. (2014) 'TopoToolbox 2 – MATLAB-based software for topographic analysis and modeling in Earth surface sciences', *Earth Surface Dynamics*, 2(1), pp. 1–7. doi: 10.5194/esurf-2-1-2014.

Seybold, H., Rothman, D. H. and Kirchner, J. W. (2017) 'Climate's watermark in the geometry of stream networks', *Geophysical Research Letters*, 44, pp. 2272–2280. doi: 10.1002/2016GL072089.

Shreve, R. L. (1967) 'Infinite Topologically Random Channel Networks', *The Journal of Geology*, 75(2), pp. 178–186.

Shulmeister, J. *et al.* (2009) 'Catastrophic landslides, glacier behaviour and moraine formation - A view from an active plate margin', *Quaternary Science Reviews*. Elsevier Ltd, 28(11–12), pp. 1085–1096. doi: 10.1016/j.quascirev.2008.11.015.

Sklar, L. S. *et al.* (2016) 'Catchment power and the joint distribution of elevation and travel distance to the outlet', *Earth Surf. Dynam*, 4(4), pp. 799–818. doi: 10.5194/esurf-4-799-2016.

Strahler, A. N. (1957) 'Quantitative Analysis of Watershed Geomorphology', *EOS, Transactions American Geophysical Union*, 38(6), pp. 913–920. doi: 10.1029/TR038i006p00913.

Sturman, A. and Wanner, H. (2001) 'A Comparative Review of the Weather and Climate of the Southern Alps of New Zealand and the European Alps', *Mountain Research and Development*, 21(4), pp. 359–369.

Sutherland, R., Davey, F. and Beavan, J. (2000) 'Plate boundary deformation in South Island, New Zealand, is related to inherited lithospheric structure', *Earth and Planetary Science Letters*, 177(3–4), pp. 141–151. doi: 10.1016/S0012-821X(00)00043-1.

Tarboton, D. G. (1996) 'Fractal river networks, Horton's laws and Tokunaga cyclicity', *Journal of Hydrology*, 187, pp. 105–117. doi: 10.1016/S0022-1694(96)03089-2.

Tarboton, D. G., Bras, R. L. and Rodriguez-Iturbe, I. (1991) 'On the extraction of channel networks from digital elevation data', *Hydrological Processes*. John Wiley & Sons, Ltd, 5(1), pp. 81–100. doi: 10.1002/hyp.3360050107.

Tarboton, D. G., Bras, R. L. and Rodriguez-Iturbe, I. (1992) 'A physical basis for drainage density', *Geomorphology*, 5(1–2), pp. 59–76. doi: 10.1016/0169-555X(92)90058-V.

Tippett, J. M. and Kamp, P. J. J. (1993) 'The role of faulting in rock uplift in the Southern Alps, New Zealand', *New Zealand Journal of Geology and Geophysics*, 36(4), pp. 497–504. doi: 10.1080/00288306.1993.9514595.

Tippett, J. M. and Kamp, P. J. J. (1995) 'Geomorphic evolution of the Southern Alps, New Zealand', *Earth Surface Processes and Landforms*, 20(1995), pp. 177–192.

Tokunaga, E. (1978) 'Consideration of the composition of drainage networks and their evolution', *Geographical Reports of Tokya Metropolitan University*, 13.

Viaplana-Muzas, M. *et al.* (2015) 'Drainage network evolution and patterns of sedimentation in an experimental wedge', *Tectonophysics*. Elsevier, 664, pp. 109–124. doi: 10.1016/J.TECTO.2015.09.007.

Walley, Y., Tunnicliffe, J. F. and Brierley, G. J. (2018) 'The influence of network structure upon sediment routing in two disturbed catchments, East Cape, New Zealand', *Geomorphology*. Elsevier, 307, pp. 38–49. doi: 10.1016/J.GEOMORPH.2017.10.029.

Willett, S. D. *et al.* (2014) 'Dynamic reorganization of river basins.', *Science*. American Association for the Advancement of Science, 343(6175). doi: 10.1126/science.1248765.

Williams, P. W. (1991) 'Tectonic geomorphology, uplift rates and geomorphic response in New Zealand', *Catena*. Elsevier, 18(5), pp. 439–452. doi: 10.1016/0341-8162(91)90048-3.

Wilson, D. D. (1989) 'Quaternary geology of Northwestern Canterbury Plains.', *Miscellanious series map 14, 1:100,000*, New Zealan. Available at: https://scholar.google.com/scholar?cluster=7437075591245989158&hl=en&oi=scholarr (Accessed: 18 August 2017).

Zanardo, S., Zaliapin, I. and Foufoula-Georgiou, E. (2013) 'Are American rivers Tokunaga self-similar? New results on fluvial network topology and its climatic dependence', *Journal of Geophysical Research: Earth Surface*, 118, pp. 166–183. doi: 10.1029/2012JF002392.

[dataset] Geographx (2012) 'NZ 8m Digital Elevation Model'. The Dominion Observatory, Wellington: LINZ - Land Information New Zealand. Available at: https://data.linz.govt.nz/layer/768.

[dataset] GNS (2012) '1:250 000 Geological Map of New Zealand (QMAP)'. Institute of Geological and Nuclear Sciences. Available at: https://www.gns.cri.nz/Home/Our-Science/Land-and-Marine-Geoscience/Regional-Geology/Geological-Maps/1-250-000-Geological-Map-of-New-Zealand-QMAP/Digital-Data-and-Downloads

[dataset] Hicks, M. D. *et al.* (2019) 'Updated suspended sediment yield estimator and estuarine trap efficiency model results'. NIWA. Available at: https://data.mfe.govt.nz/layer/103686-updated-suspended-sediment-yield-estimator-and-estuarine-trap-efficiency-model-results-2019/.

[dataset] Landcare (2015) ‘New Zealand Land Cover Database (LCDB)’. Landcare Research New Zealand Ltd. Available at: https://lris.scinfo.org.nz/layer/48423-lcdb-v41-land-cover-database-version-41-mainland-new-zealand/.

[dataset] NIWA (2015) ‘Average Annual Rainfall, 1972-2013’. New Zealand’s Environmental Reporting Series: The Ministry for the Environment and Statistics New Zealand. Available at: https://data.mfe.govt.nz/x/UEXef3.

Figures

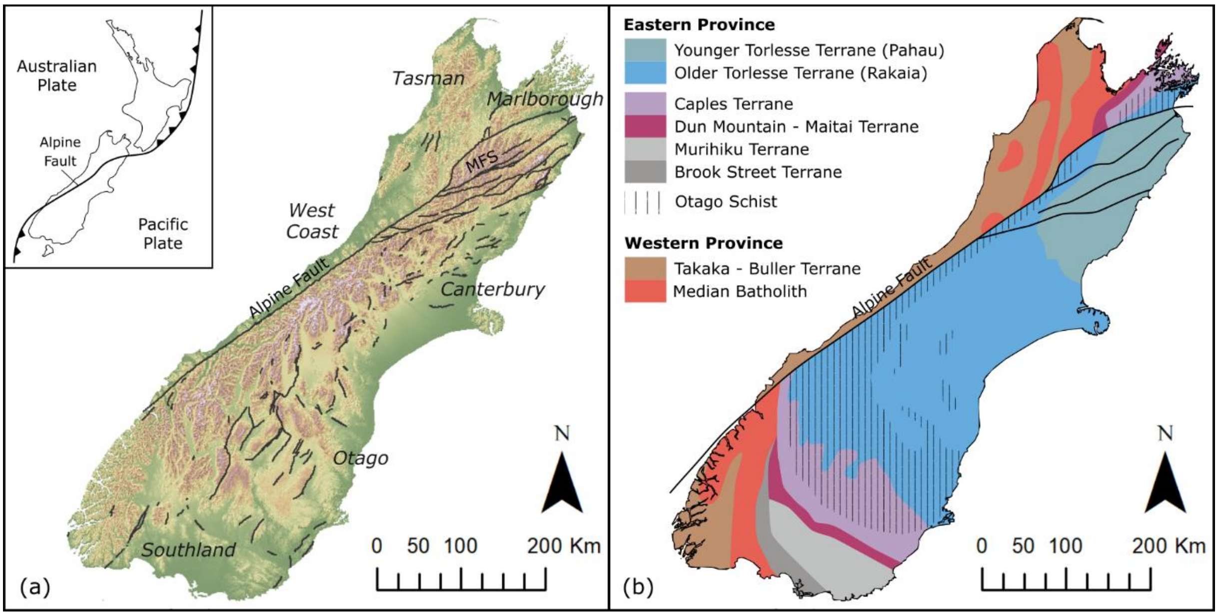

Figure 1: Topography and Geology of the South Island of New Zealand. (a) Topography and active fault lines (GNS, 2012), indicating the locations of the Alpine Fault and Marlborough Fault System (MFS). Inset map indicates the wider tectonic setting of New Zealand. (b) Basement geological terranes of the South Island, divided into the Eastern and Western Provinces.

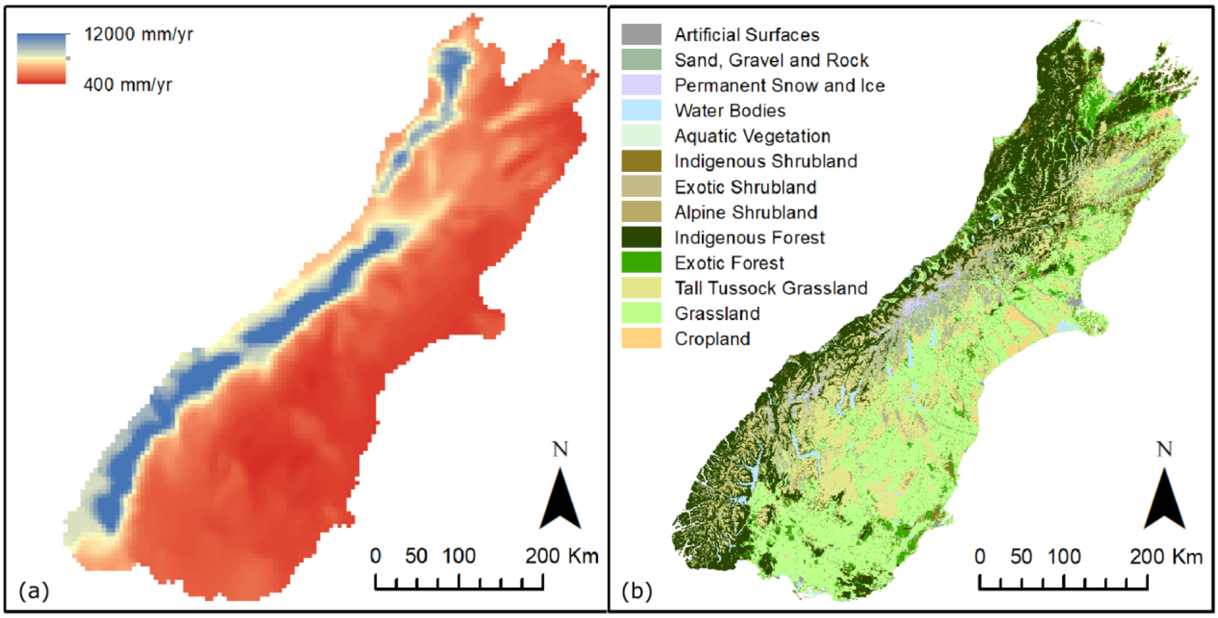

Figure 2: Rainfall and Land Cover of the South Island of New Zealand. (a) Average annual rainfall (mm/yr) (NIWA, 2015); the orographic rainfall gradient between the west and east coasts is evident, as well as the rainfall shadow in inland South Canterbury/Otago. (b) Land cover classification (Landcare, 2015); the Southern Alps dominate the landscape such that patterns of land use correspond to those of geology, relief and rainfall.

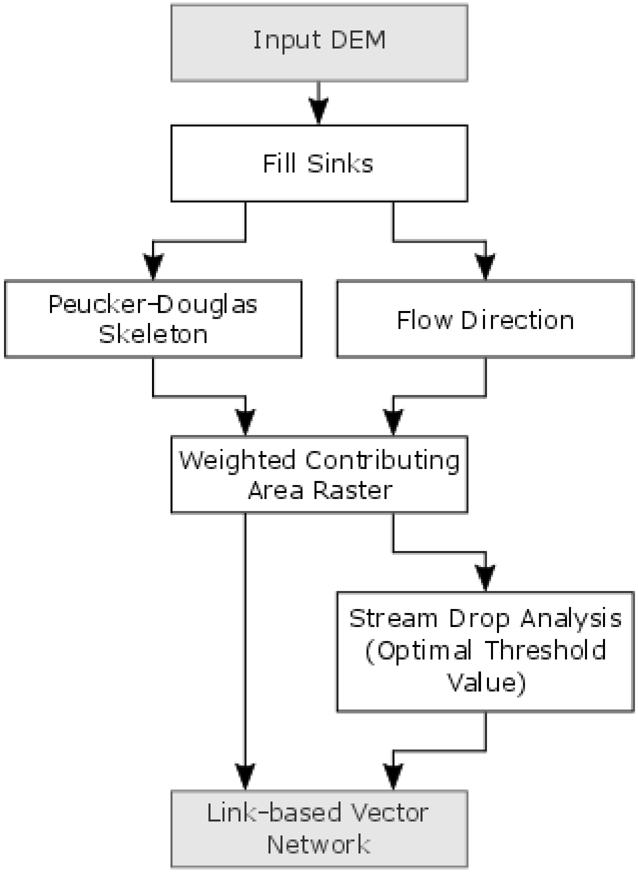

Figure 3: Method for extracting the stream networks from the DEM. The method is described by Tarboton et al. (1991, 1992) and primarily involves a Peucker-Douglas Skeleton of upwardly curving grid cells, and a stream drop analysis to define network channel heads.

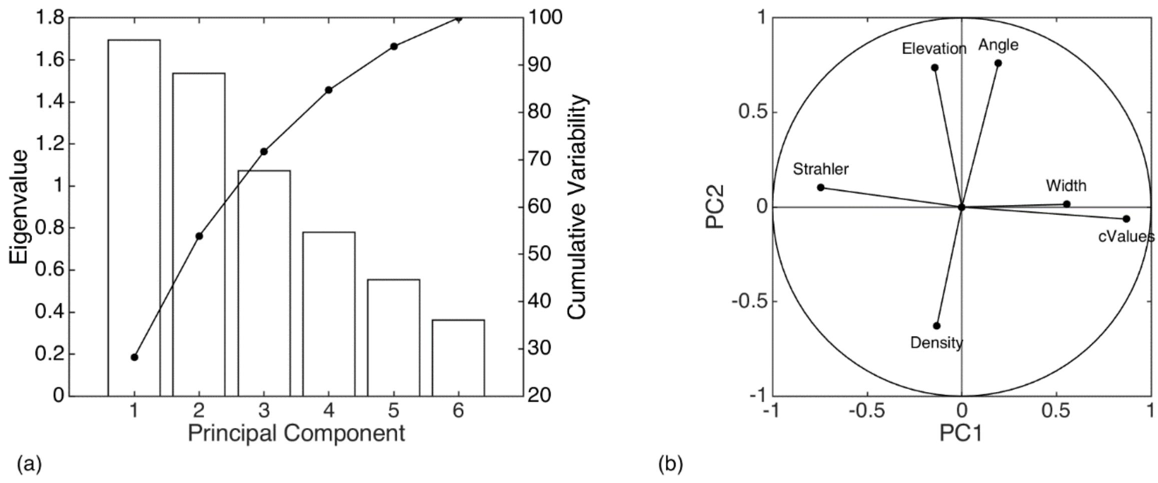

Figure 4: Results of the Principal Component analysis (PCA). (a) Scree Plot of eigenvalues and cumulative variability for each principal component, and (b) correlation between topological variables and principal components.

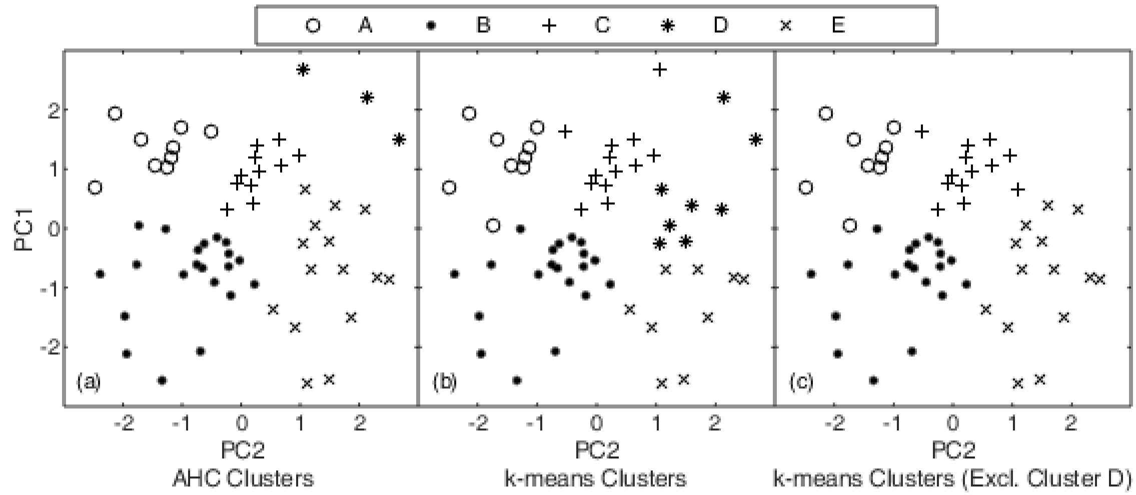

Figure 5: Distribution of catchments on the principal components, classified by, (a) AHC, (b) k-means clustering and, (c) k-means clustering excluding cluster D.

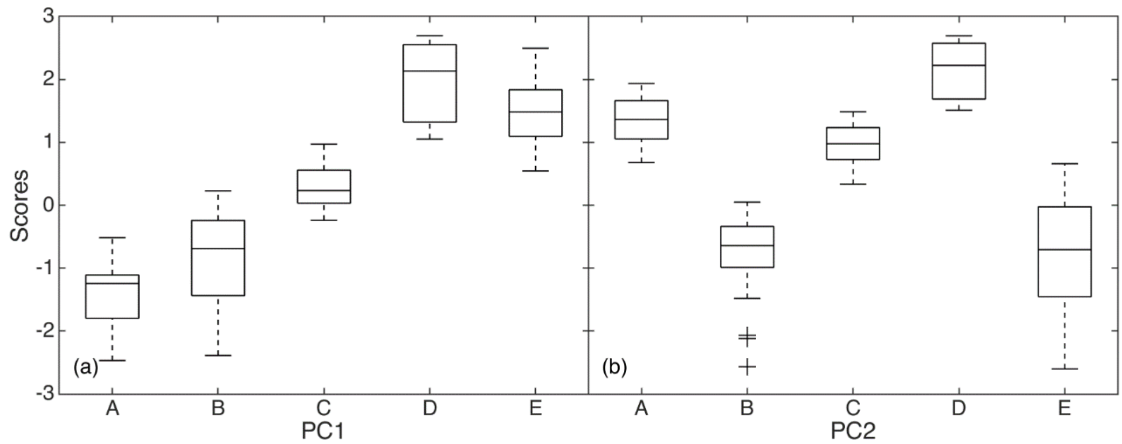

Figure 6: Box-and-whisker plots of catchment scores classified using the AHC method, along (a) principal component 1, and (b) principal component 2. Pairs of clusters with overlapping scores in PC1 (e.g. clusters A and B) do not show any overlap in PC2, indicating statistically distinct clusters.

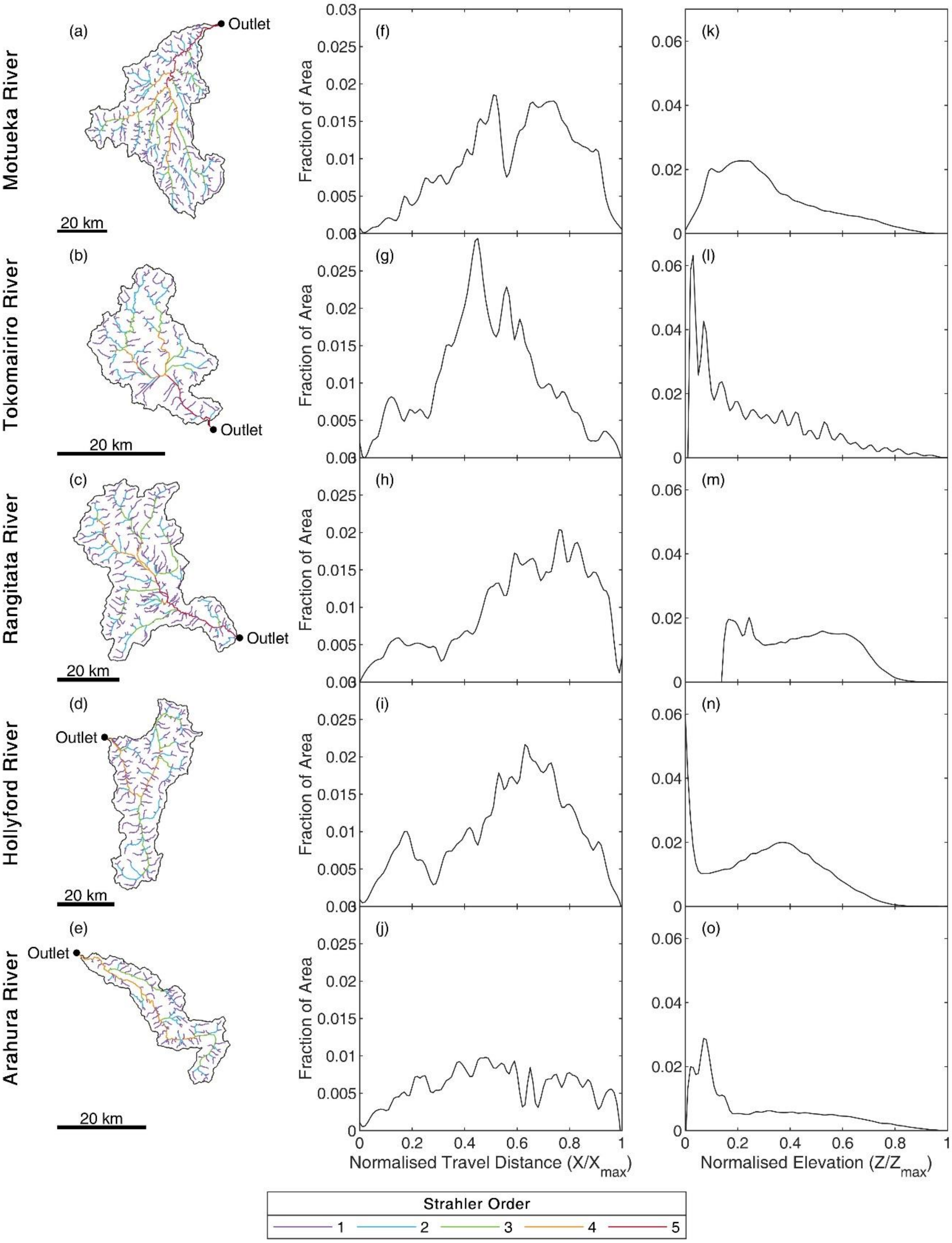

Figure 7. Internal catchment structure of the five central objects in each class. (a)-(e) Network map indicating Strahler orders, (f)-(j) Width function, a normalised frequency distribution of travel distance to the outlet, and (k)-(o) Hypsometry function, a normalised frequency distribution of elevation. Binning increments for the width and hypsometry functions were 1/50 of maximum value.

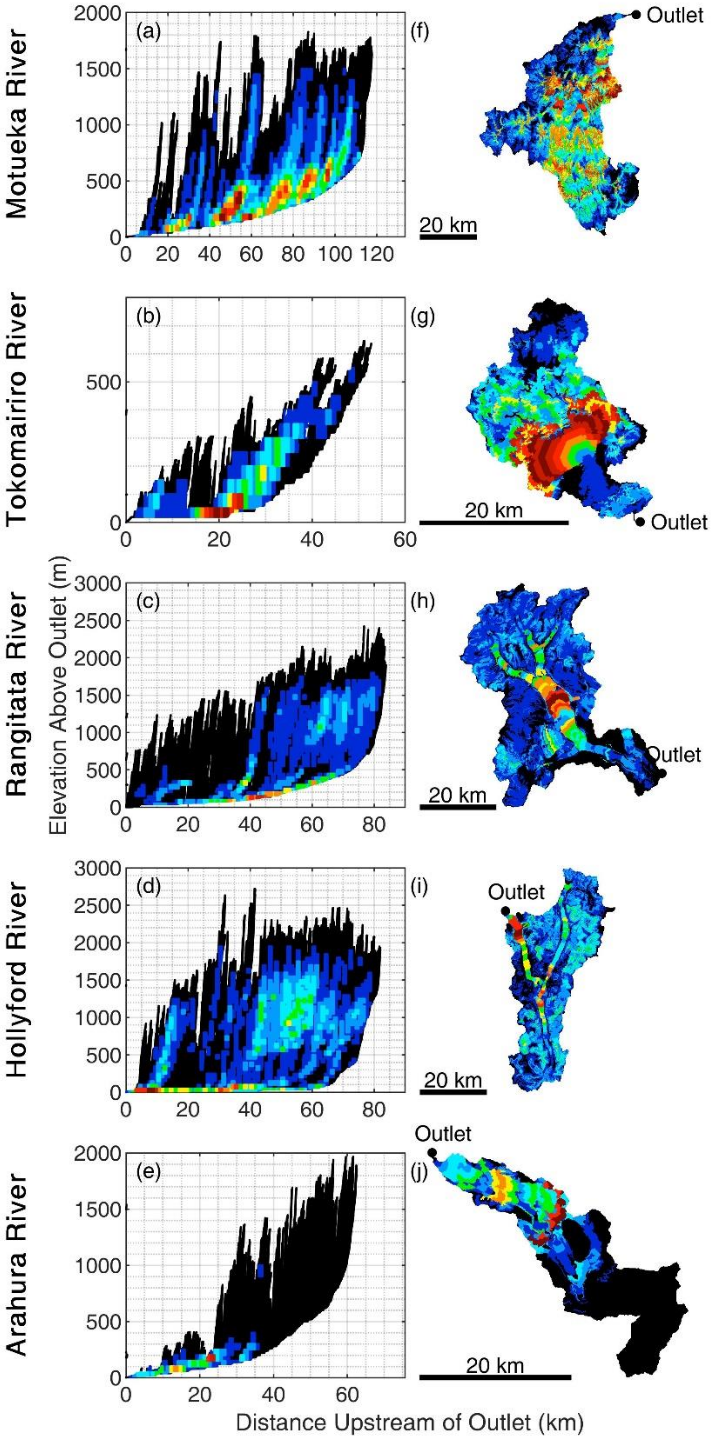

Figure 8: Distribution of Elevation and Travel Distance for (a)-(e) every point in the catchment binned in a bivariate frequency distribution, showing the relative density of cells. Panels (f)-(j) display the data from (a)-(e) as a catchment map.

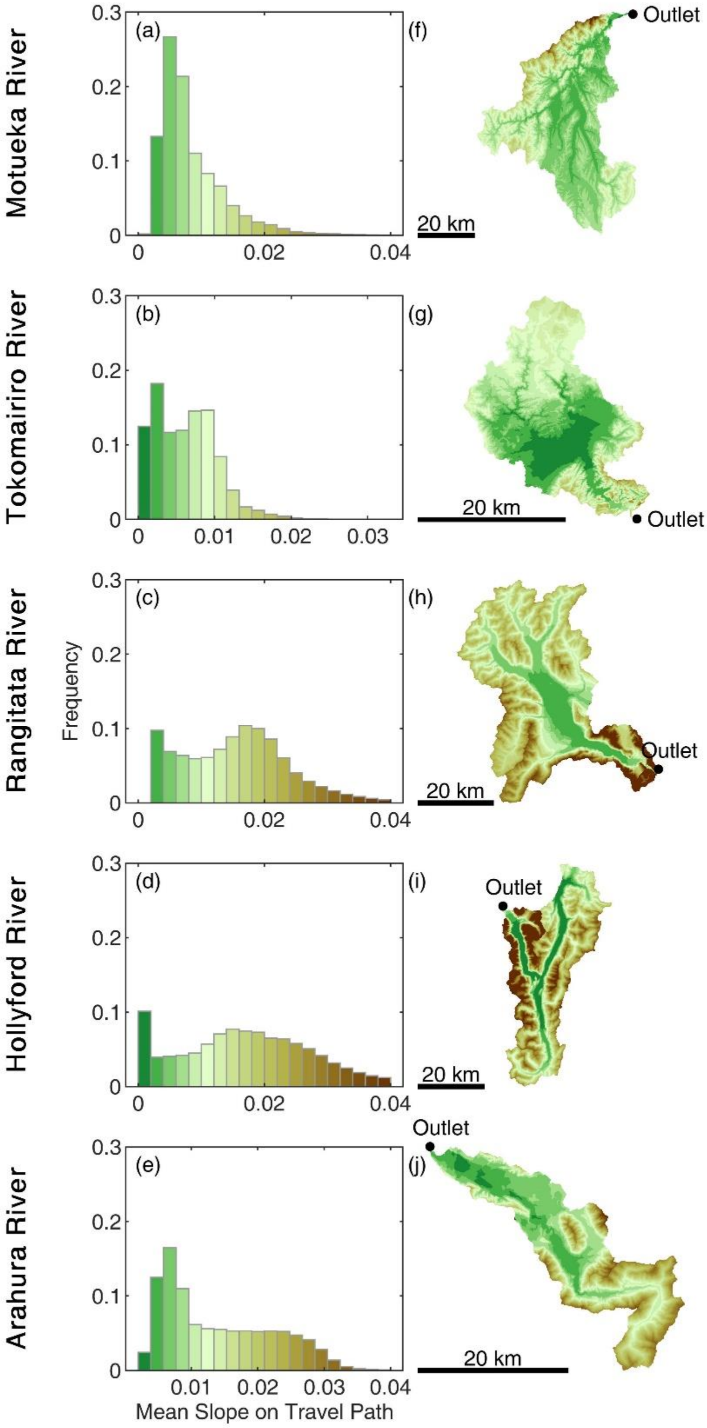

Figure 9: Distribution of mean slope. Panels (a)-(e) show histograms of mean slope along the travel path, and these are used in panels (k)-(o) to display the distribution of slope across each catchment.

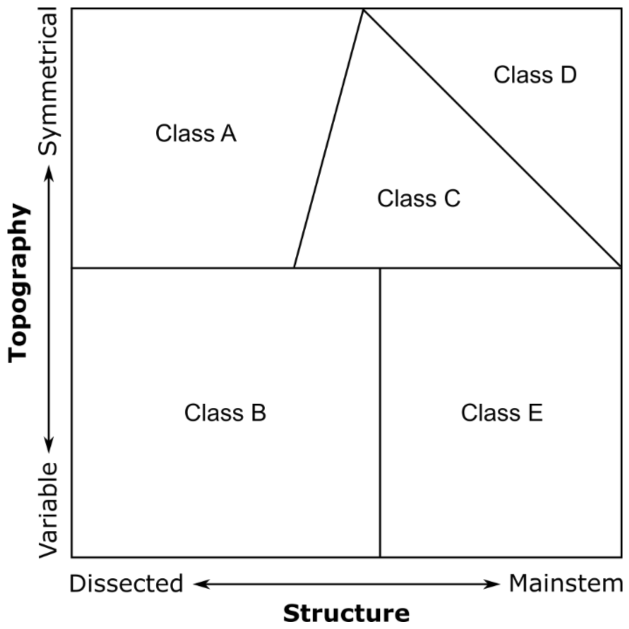

Figure 10: Simplified representation of AHC clusters in Fig. 5a, and summary characteristics of the principal components.

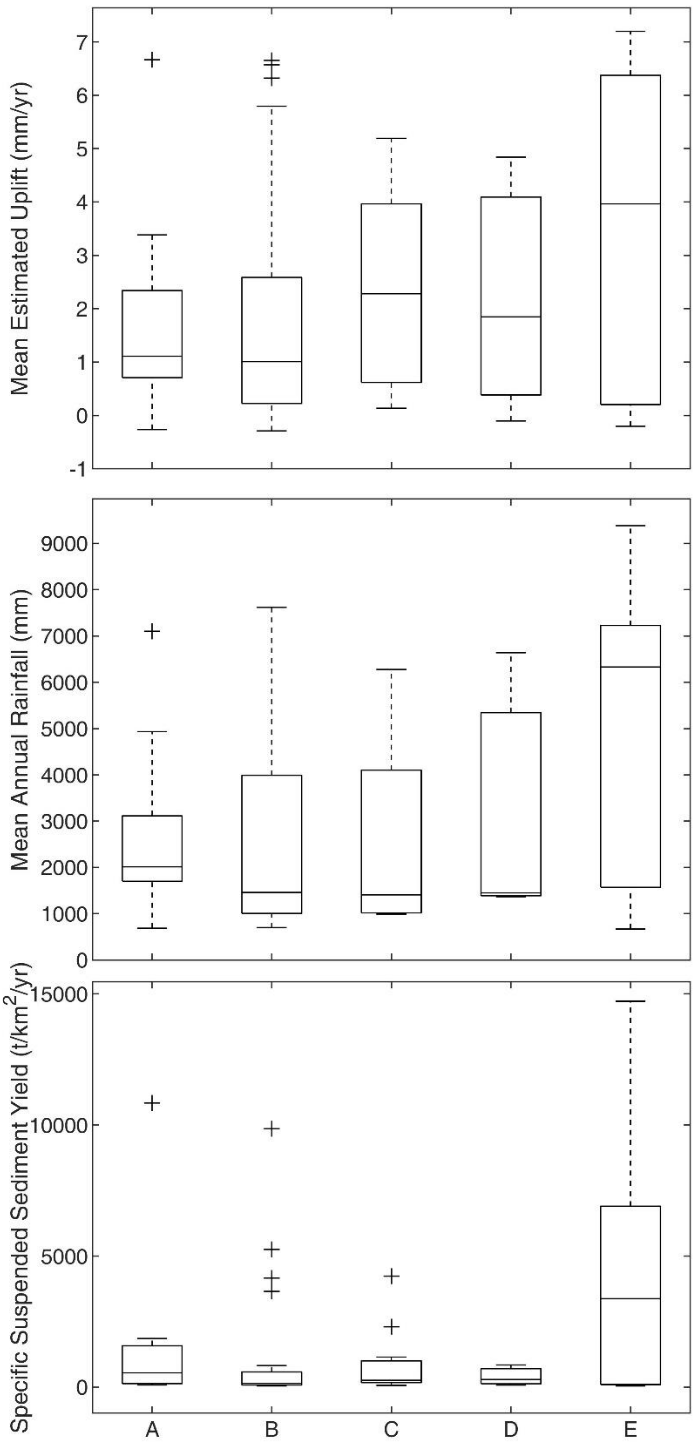

Figure 11. Box-and-Whisker plots of regional controls on network topology, for which mean values were calculated for each catchment. Regional controls include (a) estimated uplift (interpolated from approximate contours of uplift rates (Williams, 1991)), (b) average annual rainfall (NIWA, 2015) and (c) suspended sediment yield (Hicks et al., 2019).

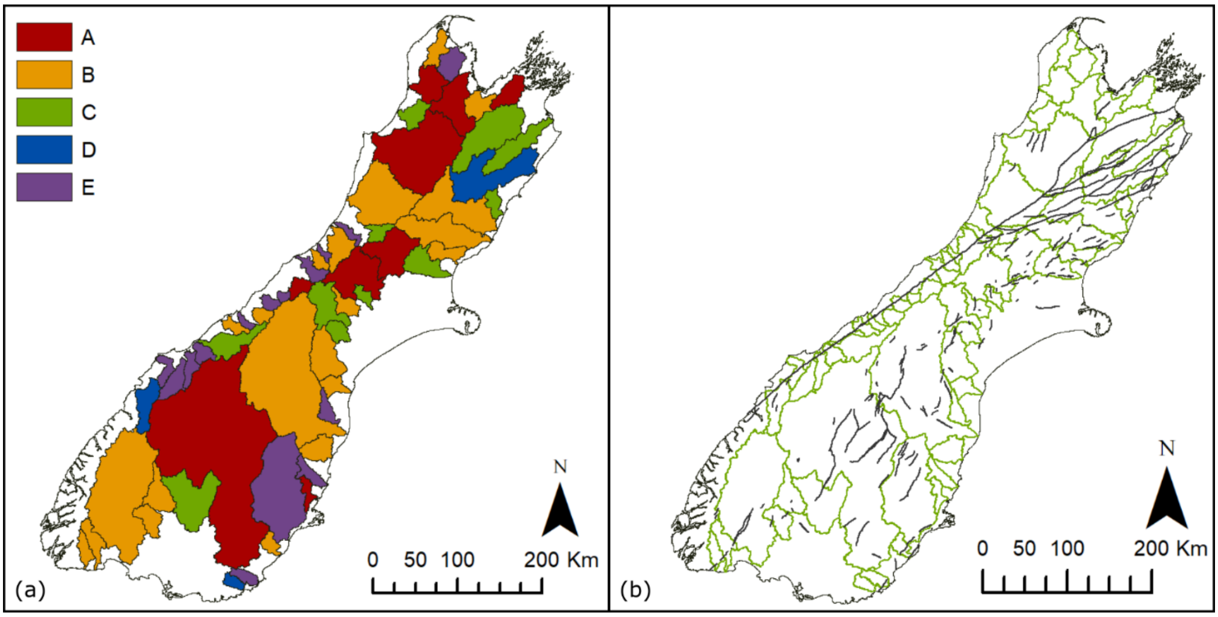

Figure 12. Regional map of study catchments, (a) classified according to the AHC clusters, and b) outlines superimposed over the locations of active faultlines.

Tables

Table 1: Parameters of network topology used in the topological classification.

Parameters	Loadings	Description	Source
Strahler Order (Ω)	-0.75 (PC1)	Value at outlet	Strahler (1957)
Network Branching (c)	0.87 (PC1)	Value at outlet	Zanardo et al. (2013) Walley et al. (2018)
Width Ratio	0.55 (PC1)	16/84 ratio of number of links per band	Heasley et al. (2019)
Elevation Ratio	0.74 (PC2)	16/84 ratio of mean elevation per band	Heasley et al. (2019)
Drainage Density (km/km^2)	-0.63 (PC2)	Total network length/catchment area	Benda et al. (2004)
Confluence Angle (°)	0.76 (PC2)	Mean of all confluences	Seybold et al. (2017)

Table 2. Parameter values summarised in each class identified by the AHC analysis.

Class	Strahler Order (Ω) *Median*	Network Branching (c)	Width Ratio	Elevation Ratio	Drainage Density (km/km^2)	Confluence Angle (°) *Mean*
A	6	Low	Wide Headwaters	Moderately Gentle	Mid	72.6
B	5	Low	Wide Headwaters and Consistent Width	Moderately Steep	High	64.5
C	5	Mid	Wide Headwaters and Consistent Width	Moderate	Mid	72.0
D	4	High	Consistent Width	Moderately Gentle	Low	78.3
E	4	High	Consistent Width	Steep	High	66.1